sensors

MDPI

Article

Fluorinated Metal Phthalocyanines: Interplay between Fluorination Degree, Films Orientation, and Ammonia Sensing Properties

Darya Klyamer [1], Aleksandr Sukhikh [1,2], Sergey Gromilov [1,2], Pavel Krasnov [3,4] and Tamara Basova [1,2,*]

1 Nikolaev Institute of Inorganic Chemistry SB RAS, Lavrentiev Pr. 3, 630090 Novosibirsk, Russia; klyamer@niic.nsc.ru (D.K.); a_sukhikh@niic.nsc.ru (A.S.); grom@niic.nsc.ru (S.G.)
2 Department of Natural Sciences, Novosibirsk State University, 2 Pirogov street, 630090 Novosibirsk, Russia
3 Institute of Nanotechnology, Spectroscopy and Quantum Chemistry, Siberian Federal University, 660041 Krasnoyarsk, Russia; kpo1980@gmail.com
4 Reshetnev Siberian State University of Science and Technology, 82 Mira prospect, 660049 Krasnoyarsk, Russia
* Correspondence: basova@niic.nsc.ru; Tel.: +7-383-330-8957

Received: 8 June 2018; Accepted: 2 July 2018; Published: 3 July 2018

Abstract: In this work, the sensor response of $MPcF_x$ (M = Cu, Co, Zn; x = 0, 4, 16) films toward gaseous NH_3 (10–50 ppm) was studied by a chemiresistive method and compared to that of unsubstituted MPc films to reveal the effects of central metals and F-substituents on the sensing properties. A combination of atomic force microscopy and X-ray diffraction techniques have been used to elucidate the structural features of thin $MPcF_x$ films deposited by organic molecular beam deposition. It has been shown that the sensor response of $MPcF_4$ films to ammonia is noticeably higher than that of MPc films, which is in good correlation with the values of binding energy between the metal phthalocyanine and NH_3 molecules, as calculated by the density functional theory (DFT) method. At the same time, in contrast to the DFT calculations, $MPcF_{16}$ demonstrated the lesser sensor response compared with $MPcF_4$, which appeared to be connected with the different structure and morphology of their films. The $ZnPcF_4$ films were shown to exhibit a sensitivity to ammonia up to concentrations as low as 0.1 ppm, and can be used for the selective detection of ammonia in the presence of some reducing gases and volatile organic compounds. Moreover, the $ZnPcF_4$ films can be used for the detection of NH_3 in the gas mixture simulating exhaled air (N_2 76%, O_2 16%, H_2O 5%, and CO_2 3%).

Keywords: metal phthalocyanines; thin films; chemiresistive sensors; ammonia; DFT calculations

1. Introduction

Ammonia is an important commercial chemical used to make fertilizers, household cleaners, and refrigerants, and is used to synthesize other chemicals. Despite its natural origin and wide distribution, ammonia is both a highly toxic and corrosive gas in its concentrated form. It is classified as an extremely hazardous substance, and is subjected to strict monitoring of its concentration in the environment, as well as in the automotive and chemical industry [1]. The detected concentration levels of ammonia depend on the application areas and can be varied in a very wide range, from ppb to hundreds ppm [1].

Recently, interest has been escalating into the study of exhaled breath as a noninvasive method of diagnostics for bronchopulmonary, cardiovascular, gastrointestinal, and other diseases [2]. Inference can be made regarding the changes in the metabolism and about the presence of a particular disease according to changes in the ratios of substances released in human breath. For example, an ammonia concentration of

>1 ppm indicates renal failure in nephritis, atherosclerosis of the renal arteries, toxic affections of kidneys, and other diseases [3].

There are several ammonia detection devices described in the literature. Among those, optical gas analyzers [4–6], catalytic ammonia sensors [1], metal-oxide gas sensors [7,8], conducting polymer gas detectors [9–11], and chemiresistive sensors based on carbon nanomaterials and two-dimensional (2D) transition metal dichalcogenides [12] are used for the detection of gaseous ammonia, with their virtues and shortcomings. Electrolytic devices usually suffer from their low detection limits and limited accuracy, while optical sensors have very good sensitivity, but they are usually suited only for laboratory testing rather than for low cost portable sensors. Conducting polymer-based sensors generally suffer from irreversible sensor response and low selectivity in the presence of other gases [13].

Thin films of metal phthalocyanine (MPc) derivatives and their hybrid materials are of considerable interest as active layers of chemiresistive sensors for ammonia detection [14,15]. The introduction of various substituents into the phthalocyanine macrocycle can significantly alter the films' structure and morphology, and in turn, leads to a change of their electrical and sensing properties [15,16]. Fluorine substituents decrease the electron density of the aromatic ring and increase the oxidation potential of the MPc molecule [17]. As a result, fluorosubstituted phthalocyanines exhibit a higher sensor response to reducing gases, such as ammonia and hydrogen [18]. The better sensor response of the $ZnPcF_{16}$ and $PdPcF_{16}$ films towards gaseous ammonia compared with their unsubstituted analogues was presented by Schollhorn et al. [19,20] and Klyamer et al. [15], respectively. To the best of our knowledge, only sporadic data on the structural features and sensing behavior of tetrafluorosubstituted metal phthalocyanine ($MPcF_4$) films are available in the literature [15,16,21]. In our previous work [15], we studied the structure of $CoPcF_4$ films deposited by thermal evaporation and their sensor response to ammonia. It has been shown that, similarly to the case of $MPcF_{16}$, the sensor response to ammonia is noticeably higher compared with unsubstituted CoPc films. To the best of our knowledge, the systematic analysis of the interplay between the fluorination degree, films' orientation, and sensing properties have never been carried out in the literature.

In this work, the sensor response of $MPcF_x$ (M = Cu, Co, Zn; x = 4, 16) films toward gaseous NH_3 (10–50 ppm) was studied by the chemiresistive method and compared to that of unsubstituted MPc films to reveal the effects of central metals and F-substituents on the sensing properties. A combination of atomic force microscopy and X-ray diffraction techniques have been used to elucidate the structural features and molecular orientation of thin films of $MPcF_x$ deposited by organic molecular beam deposition. Density functional theory (DFT) calculations have been performed to estimate the probable structure of $MPcF_x$-analyte complexes and their bond formation energies. The sensor characteristics of $ZnPcF_4$ films were studied in more detail to demonstrate their application for the selective detection of a low concentration of ammonia (up to 0.1 ppm) in the presence of CO_2 and water vapors, as well as in the gas mixture with the composition close to exhaled air (N_2 76%, O_2 16%, H_2O 5%, and CO_2 3%).

2. Materials and Methods

2.1. Preparation and Study of Thin Films

Unsubstituted (MPc, M = Cu, Co, Zn), tetrafluorosubstituted ($MPcF_4$, M = Cu, Co, Zn), and hexadecafluorosubstituted ($MPcF_{16}$, M = Cu, Co, Zn) phthalocyanines were synthesized, according to the procedures described elsewhere [15,16], from the corresponding phthalonitrile derivatives and corresponding metal chlorides. $MPcF_4$ derivatives were prepared as a statistical mixture of four regioisomers because of the various possible positions of the fluorine substituents. The isomers were not separated because of the close parameters of sublimation.

The thin films of all of the investigated phthalocyanines were deposited by an organic molecular beam deposition under a vacuum of 10^{-5} Torr, onto platinum interdigitated electrodes (Dropsens, Oviedo, Spain). The electrodes have the following dimensions: the gap between digits is 10 μm; number of digits is 125 × 2 with a digit length of 6760 μm; and cell constant is 0.0118 cm^{-1}. The nominal thickness of the phthalocyanine films was about 100 nm.

XRD studies of the thin film samples were carried out using a Shimadzu XRD-7000 diffractometer (CuKα, λ = 1.54187Å, Bragg–Brentano scheme, θ-θ goniometer, copper anode sealed tube 30 mA@40 kV with a Ni filter and scintillation counter detector). The scan range was from 5° to 30° 2θ, with the step of 0.03°, and the acquisition time of 40 s per step. The atomic force microscopy (AFM) in the tapping mode with a Nanoscope IIIa (Veeco Instruments, Plainview, NY, USA) scanning probe microscope was used for the characterization of the films' morphology.

To test the chemiresistive sensor response the films were put into the flow cell and held for 10 min under air flow until the resistance reached a steady state value. Then NH_3 gas (0.1–50 ppm) was diluted with air and injected. Air was used as the dilution and carrier gas. The electrical resistance of phthalocyanine films was measured with a Keithley 236 electrometer by applying a constant dc voltage (8 V). All gas sensing measurements were carried out at room temperature.

2.2. Theoretical Calculations

The interaction of MPc, $MPcF_4$, and $MPcF_{16}$ with NH_3 was studied by the density functional theory (DFT), using the BP86/def2-SVP method [22–25] and the Grimme D3 dispersion correction [26,27]. The ORCA suite of the quantum chemical programs was used for all of the calculations [28].

The binding energy (E_b) was calculated according to the Equation (1), as a difference of the total energies of the corresponding adduct and its interacting components, as follows:

$$E_b = E_{\mathrm{CoPcF}_x-\mathrm{NH}_3} - E_{\mathrm{NH}_3} - E_{\mathrm{CoPcF}_x} \tag{1}$$

The effective charge $q(NH_3)$ was calculated according to the Equation (2), as follows:

$$q = \sum_n \left(Z_n - \sum_{I \in n} \sum_J P_{IJ} S_{IJ} \right) \tag{2}$$

where Z_n is the nuclear charge of the atom n; and P_{IJ} and S_{IJ} are the elements of the density and overlap the matrixes corresponding to the atomic orbitals I and J. This scheme, realized in ORCA, is based on the widely used Mulliken population analysis [29,30]. A bond order was estimated using Mayer's method [31,32].

3. Results and Discussion

3.1. Experimental Study of the Dependence of Sensing Response on Phthalocyanine Molecular Structure

The sensor response of $MPcF_x$ (M = Cu, Co, Zn; x = 4, 16) films was studied by a chemiresistive method. The choice of phthalocyanines of copper, cobalt, and zinc was determined by their better sensitivity to ammonia, according to the experimental data and DFT calculations performed earlier by Liang et al. [33]. The change of the film resistance during the sequential injection of the gas analyte and air purging was measured. The typical sensor response toward ammonia is shown in Figure 1, using $CoPcF_4$ and $CoPcF_{16}$ (b) films as an example.

The introduction of ammonia to the gas cell leads to the increase of resistance of the CoPc and $CoPcF_4$ films. Similar behavior typical of organic semiconductor films possessing p-type conductivity [34] was also observed in the case of ZnPc, CuPc, $ZnPcF_4$, and $CuPcF_4$ films.

The resistance-based sensing mechanism of the semiconducting sensors has been studied in the literature [35,36]. It has been reported that the formation of the charge-transfer complexes by the coordination of O_2 to MPc, at the air/phthalocyanine interface and at the grain boundaries, leads to the formation of oxidized MPc^+ and O^{2-} species, and the injection of hole charge carriers into the films' bulk [37,38]. When a p-type semiconductor gas sensor is exposed to the reducing NH_3 gas, the electrons injected into the material through the oxidation reaction between the reducing gas and the O^{2-} species on the semiconductor surface decrease the concentration of the holes in the layer, which in turn increases the resistance of the MPc films [39].

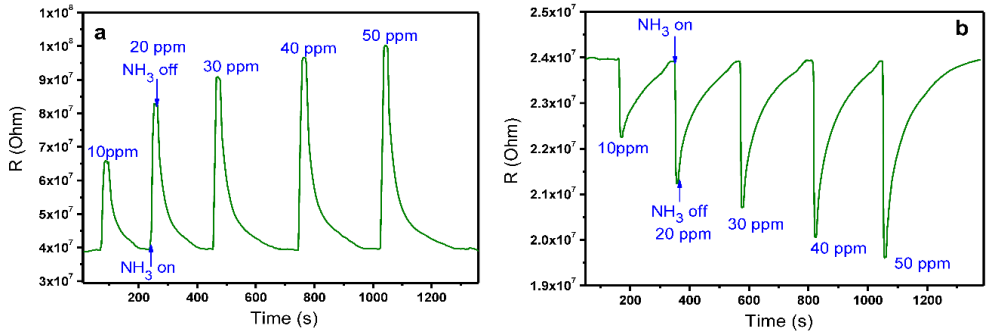

Figure 1. Sensor response of $CoPcF_4$ (**a**) and $CoPcF_{16}$ films (**b**) to ammonia (10–50 ppm).

On the contrary, the $MPcF_{16}$ (M = Co, Cu, Zn) films exhibit a decrease of their resistance upon interaction with the electron donor NH_3 molecules. It is known that perfluorinated metal phthalocyanines demonstrate the n-conducting behavior because of the effect of the electron-withdrawing fluorine substituents [40,41]. When an n-type semiconductor gas sensor is exposed to the reducing NH_3 gas, ionized oxygen anions are used to oxidize the reducing gas, and the released electrons inject into the semiconducting core, which decreases the sensor resistance proportionally to the concentration of the reducing gas-analyte [36].

To study the influence of the phthalocyanine molecular structure on the sensing behavior, the sensor responses of the $MPcF_x$ (M = Co, Cu, Zn; x = 0, 4, 16) films toward ammonia were compared in the concentration range from 10 to 50 ppm. Figure 2 shows the dependence of the relative sensor response $R_n = |R\text{-}R_o|/R_o$ (where R is the resistance at a certain concentration of the analyte, R_o is the resistance before injection of the analyte vapors) for the MPc, $MPcF_4$, and $MPcF_{16}$ films. It can be seen that the sensor response decreases in the order of $CoPcF_x$ > $ZnPcF_x$ > $CuPcF_x$, both in the case of the unsubstituted (Figure 2a) and fluorinated derivatives (Figure 2b,c). For instance, the sensor response of the CoPc films toward 10 ppm of ammonia is about two times higher compared with the ZnPc films, and eight times higher compared with the CuPc films (Figure 2a). An even more pronounced difference is observed in the case of the $MPcF_4$ and $MPcF_{16}$ films, for example, the sensor response of the $CoPcF_x$ (x = 4, 8) films toward 10 ppm of ammonia is about four times higher compared with the $ZnPcF_x$ films, and 13 times higher compared with the $CuPcF_x$ films (Figure 2b,c).

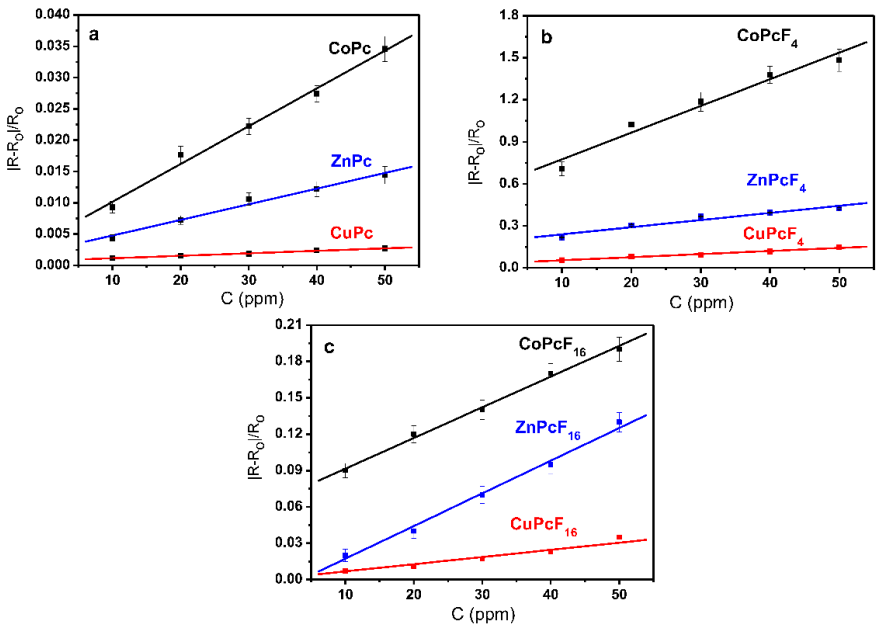

Figure 2. Dependence of the relative sensor response $|R\text{-}R_o|/R_o$ on NH_3 concentration (10–50 ppm) for MPc (**a**); $MPcF_4$ (**b**), and $MPcF_{16}$ (**c**) (M = Zn, Co, Cu) films.

Figure 3 demonstrates the effect of the F-substitution in the phthalocyanine ring on the sensing response to ammonia, using the $ZnPcF_x$ (x = 0, 4, 16) films as an example. The sensor response decreases in the order of $ZnPcF_4$ > $ZnPcF_{16}$ > ZnPc. The same order is also observed for the $CuPcF_x$ and $CoPcF_x$ films. The $MPcF_4$ films exhibit the maximal sensor response to ammonia among all of the investigated phthalocyanines, for example, the sensor response of the $MPcF_4$ (M = Zn, Co, Cu) films is 3–10 times higher than that of the $MPcF_{16}$ films, and 30–70 times higher than that of the MPc films. Therefore, the introduction of the F-substituents to the phthalocyanine macrocycle leads to a substantial increase of their sensitivity to ammonia.

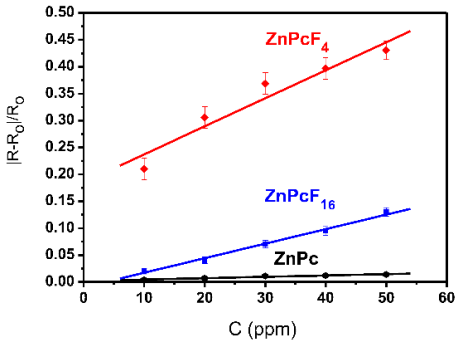

Figure 3. Dependence of the sensor response $|R-R_o|/R_o$ on NH_3 concentration (10–50 ppm) for ZnPc, $ZnPcF_{16}$, and $ZnPcF_4$ films.

The plots of dependencies of the response and recovery times on NH_3 concentration (10–50 ppm) for the $ZnPcF_x$ (a), $CoPcF_x$ (b), and $CuPcF_x$ (c) (x = 0, 4, 16) films are shown in Figure 4. The average values of the response and recovery times of all of the investigated films are also given in Table 1. All of the investigated films exhibited a reversible sensor response at room temperature, with the response time of 10–25 s. The maximal recovery times are observed in the case of the $CoPcF_x$ films, and decrease in the order of $CoPcF_x$ > $ZnPcF_x$ > $CuPcF_x$. This order correlates with the energy of the binding of $MPcF_x$ with analyte molecules, as shown below in the Section 3.2. The more binding energy between $MPcF_x$ and NH_3, the higher the value of recovery time is observed.

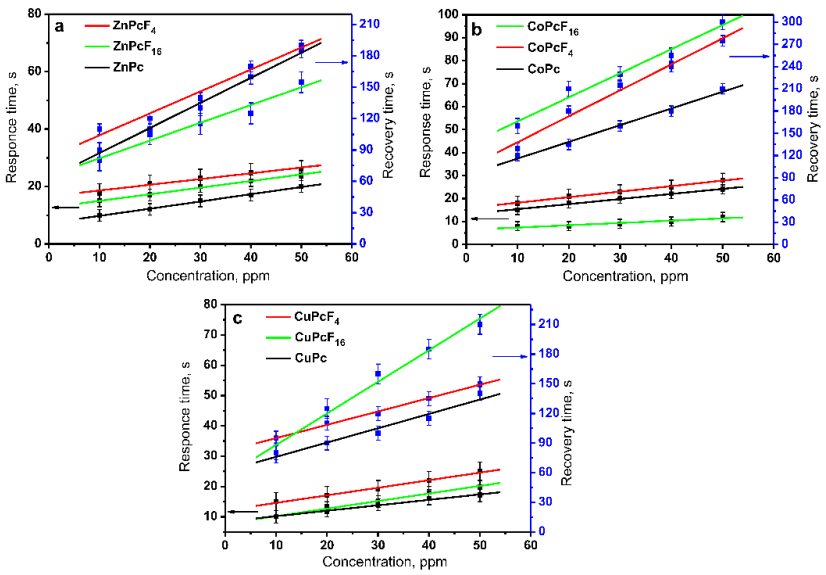

Figure 4. Dependence of the response and recovery times on NH_3 concentration (10–50 ppm) for $ZnPcF_x$ (**a**), $CoPcF_x$ (**b**), and $CuPcF_x$ (**c**) (x = 0, 4, 16) films.

Table 1. Average values of response and recovery times of MPc, $MPcF_4$, and $MPcF_{16}$ films at the concentration of ammonia 10 ppm.

Time, s	CoPc	$CoPcF_4$	$CoPcF_{16}$	ZnPc	$ZnPcF_4$	$ZnPcF_{16}$	CuPc	$CuPcF_4$	$CuPcF_{16}$
Response	15	20	10	10	25	15	10	15	10
Recovery	120	130	160	90	110	85	80	95	80

The sensor response of the sensing layers depends on several factors, among them are the molecular structure of sensing material that governs the nature and strength of its interaction with an analyte, and the sensing layer structure and morphology that determines the number of active sites, and the rate of adsorption–desorption process.

3.2. Theoretical Study of the Dependence of Sensor Response on the Phthalocyanine Molecular Structure

The DFT calculations have been performed to study the interaction of the NH_3 molecules with $MPcF_x$, and to elucidate the different sensor responses of $MPcF_x$ with different x and central metals. To check the validity of the theoretical model, the calculated vibrational spectra of $MPcF_x$ were compared with the experimental ones, as it has already been described elsewhere [15].

The most favorable structure of the MPc····NH_3 aggregates simulated by the DFT calculations was that with the NH_3 molecule binding with phthalocyanine, via its central metal. The binding of $MPcF_x$ with the NH_3 molecule increases the out-of-plane distortion of the Pc ring (e.g., the out-of-plane displacement of the Zn atom in $ZnPcF_4$ leads to an increase in the Zn-N_α bond length from 2.007 Å to 2.043 Å, on average). The binding parameters for NH_3 with $MPcF_x$ are presented in Table 2 for comparison. It has already been shown elsewhere [15,42] that the ammonia and MPcs form complexes with a charge transfer from the NH_3 to phthalocyanine molecule, via the interaction of NH_3 with the central metal ion inside the phthalocyanine macrocycle.

Table 2. Parameters of binding of NH_3 with MPc, $MPcF_4$, and $MPcF_{16}$.

Aggregate	E_b, eV	Bond Order	d, Å	$q(NH_3)$, e
CoPc····NH_3	−1.14	0.484	2.153	0.243
$CoPcF_4$····NH_3	−1.16	0.486	2.152	0.245
$CoPcF_{16}$····NH_3	−1.20	0.491	2.151	0.250
ZnPc····NH_3	−1.06	0.402	2.159	0.214
$ZnPcF_4$····NH_3	−1.08	0.405	2.156	0.216
$ZnPcF_{16}$····NH_3	−1.14	0.414	2.151	0.223
CuPc····NH_3	−0.62	0.291	2.330	0.156
$CuPcF_4$····NH_3	−0.63	0.293	2.329	0.158
$CuPcF_{16}$····NH_3	−0.68	0.302	2.322	0.164

The formation of this bond is based on the displacement of electron density from NH_3 molecule to MPc, through the central metal atom and, as a result, NH_3 acquires a positive effective charge increasing in the order of CuPc < ZnPc < CoPc, both for the unsubstituted and fluorinated derivatives (Table 2). At the same time, the M–NH_3 bond order increases, and the respective distance d between the metal atom and the ammonia nitrogen atom decreases in the same order. The obtained theoretical data are in a good correlation with the experimental investigations of the sensor response of MPc (M = Cu, Zn, Co), which is higher in the case of cobalt phthalocyanines.

As for the effect of the F-substituents, the binding energy between NH_3 and $MPcF_x$ and the positive effective charge of NH_3 increases in the order of MPc····NH_3 < $MPcF_4$····NH_3 < $MPcF_{16}$····NH_3 (Table 2). The experimental investigations of the sensor response of the unsubstituted and fluorinated phthalocyanines showed that its value is higher in the case of $MPcF_4$. However, it is necessary to mention that, in contrast to the theoretical calculations, the experimental sensor response of the $MPcF_4$ films is higher than that of $MPcF_{16}$ films. It is conceivable that such behavior can be associated with

different semiconductor properties and the mechanisms of conductivity of the $MPcF_4$ and $MPcF_{16}$ films. It has already been mentioned above that the $MPcF_4$ films possess the *p*-type conductivity, whereas the $MPcF_{16}$ films demonstrate the *n*-conducting behavior. One more important factor governing the sensing properties is the structure and morphology of the sensing layers.

3.3. Characterization of Thin Films

To study the effect of fluorination, the structure and morphology of the $MPcF_x$ films were investigated by XRD and AFM methods. X-ray diffraction patterns of thin films of all nine phthalocyanine derivatives are shown in Figure 5. The diffraction patterns contain a single strong diffraction peak in the range from 5° to 7° 2θ and several barely visible peaks with the corresponding interplanar distances *d*, which are the natural fractions of the d_0 of the strong peak. This type of diffraction patterns is a typical feature of thin films with a strong preferred orientation. Comparing the interplanar distances with the calculated ones known from the single crystal data [43,44], the CoPc and CuPc thin films were identified as metastable α-polymorphs. There are no known structural data for α-ZnPc, however, some works show that α-ZnPc is isostructural to α-CuPc and α-CoPc, and it forms when deposited onto the substrate surface at temperatures lower than 100 °C [45].

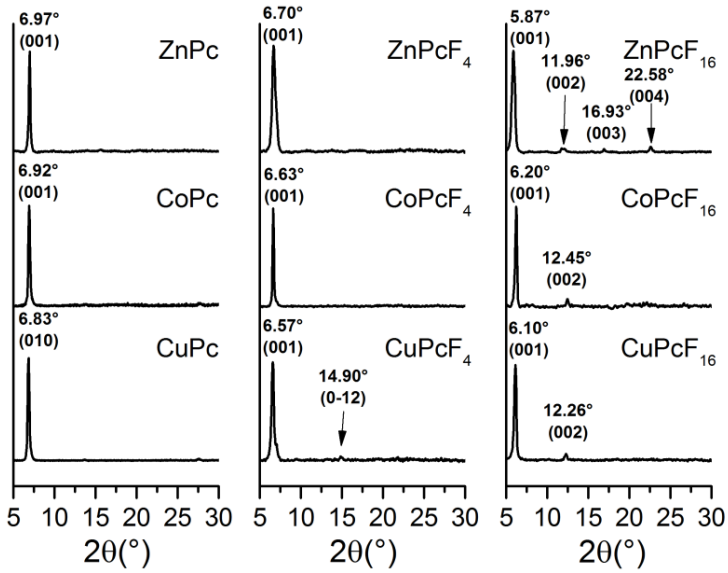

Figure 5. XRD patterns for thin film samples of $MPcF_x$ (M = Zn, Co, Cu; x = 0, 4, 16).

$CuPcF_4$, $CoPcF_4$, and $ZnPcF_4$ are isostructural with $PdPcF_4$ [16], and crystallize only in one triclinic (P-1 space group) phase. There are two known polymorphs for $CuPcF_{16}$, that is, α-$CuPcF_{16}$ (P-1 space group, Z = 1) [46] and triclinic β-$CuPcF_{16}$ (P-1 space group, Z = 2) [47], and both of them have very similar values of interplanar distances for the first peak on the calculated diffraction pattern. α-$CuPcF_{16}$ grows on the substrate surface at room temperature, while the β-$CuPcF_{16}$ are obtained at 360 °C. As, in this work, the substrate temperature was about 20 °C, it is reasonable to assume that the $CuPcF_{16}$ thin films consists of a α-phase. No crystal structure data are known for the α-polymorphs of $CoPcF_{16}$ and $ZnPcF_{16}$, but as α-CuPc/α-CoPc, $CuPcF_4$/$CoPcF_4$/$ZnPcF_4$, and β-$CuPcF_{16}$/β-$CoPcF_{16}$/β-$ZnPcF_{16}$ are isostructural to each other, we assumed that the $CoPcF_{16}$ and $ZnPcF_{16}$ thin films are also α-polymorphs, with the same structure as α-$CuPcF_{16}$.

Figure 6 shows the AFM images of the surface of the ZnPc (a), $ZnPcF_4$ (b), and $ZnPcF_{16}$ (c) films. As can be clearly seen, the ZnPc films surface consists of roundish grains (Figure 6a) and has the rms roughness value of 14.2 nm. The $ZnPcF_4$ film, having an rms roughness of 6.7 nm, is formed by azimuthally disordered elongated grains (Figure 6b). The $ZnPcF_{16}$ films exhibit a high density of

azimuthally disordered roundish grains, with the size noticeably smaller than those of the ZnPc films and the minimal rms roughness values (4.2 nm) among the investigated films (Figure 6c). The more rough and inhomogeneous surface of the $ZnPcF_4$ films can also be responsible for their higher sensor response to ammonia, compared with $ZnPcF_{16}$ films.

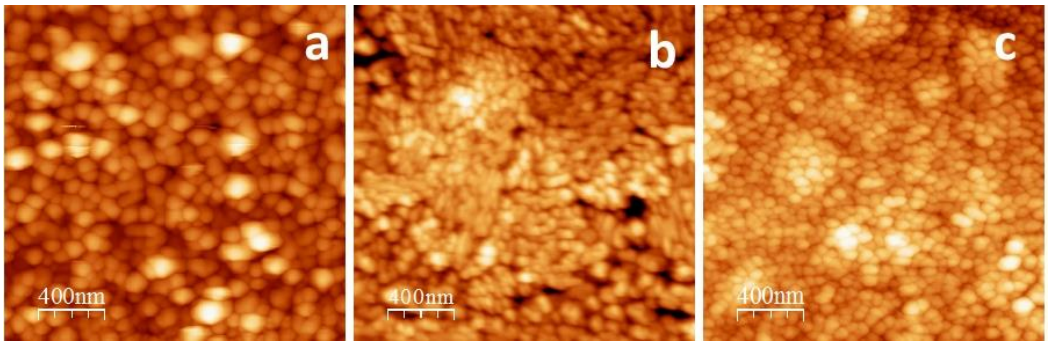

Figure 6. AFM images of ZnPc (**a**); $ZnPcF_4$ (**b**); and $ZnPcF_{16}$ (**c**) films.

3.4. Sensor Characteristics of Phthalocyanine Films

The sensor characteristics of the $MPcF_4$ films demonstrating the best sensitivity to ammonia among the investigated samples were studied in more detail to demonstrate their applicability for the detection of NH_3 at lower concentrations, down to 0.1 ppm, in the presence of other gases. A typical sensor response of a $ZnPcF_4$ layer toward ammonia, in the concentration range from 1–4 ppm, is shown in Figure 7a. To demonstrate the possible application of $ZnPcF_4$ films for the detection of gases-biomarkers in exhaled air, the sensor response of $ZnPcF_4$ films to ammonia was also tested in a mixture of gases, with the composition close to the exhaled air of healthy people. For this purpose, small amounts of ammonia (1–4 v.%) were added to the preliminarily prepared gas mixture (N_2—76%, O_2—16%, H_2O—5%, CO_2—3%). The sensor response of $ZnPcF_4$ films to ammonia (1–4 ppm) diluted with the mixture of gases N_2 76%, O_2 16%, H_2O 5%, and CO_2 3% is shown in Figure 7b.

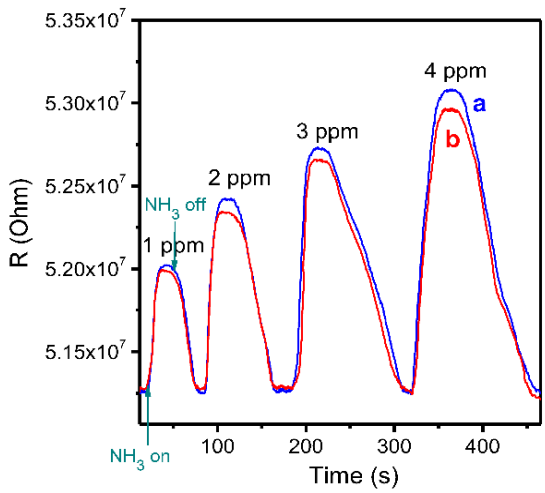

Figure 7. Sensor response of a $ZnPcF_4$ layer toward ammonia in the concentration range from 1 to 4 ppm, in air (**a**) and in a mixture of gases with the composition close to exhaled air of healthy people (N_2—76%, O_2—16%, H_2O—5%, and CO_2—3%) (**b**).

The $ZnPcF_4$ films demonstrate a reversible sensor response in the investigated concentration range, with a quite good response and recovery time; the response time varied from 15 s to 30 s,

depending on the NH_3 concentration, while the recovery time increased from 28 s to 90 s when the NH_3 concentration changes from 1 to 4 ppm. The dependence of the sensor response on the NH_3 concentration is given in Figure 8. The minimum detected concentration of NH_3 in the case of $ZnPcF_4$ films was found to be 0.1 ppm.

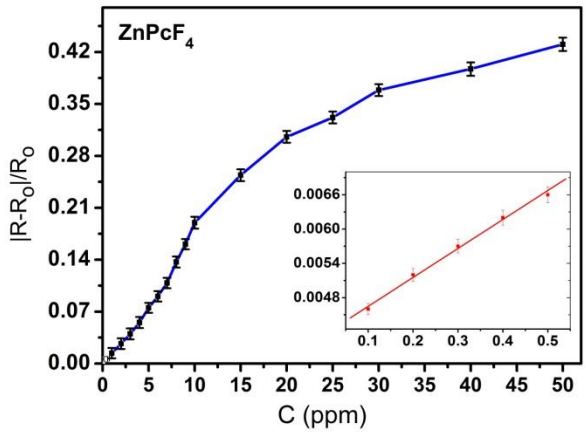

Figure 8. Dependence of the sensor response of $ZnPcF_4$ films on NH_3 concentration (0.1–50 ppm).

To study the selectivity of $ZnPcF_4$-based sensors, their response was tested against ammonia (10 ppm), acetone (1000 ppm), dichloromethane (10^4 ppm), carbon dioxide (10^4 ppm), and ethanol (10^4 ppm). Figure 9a shows that the sensor exhibited a significantly higher response to ammonia in comparison with that toward the other investigated analytes. This obviously indicates the viability of this type of sensors to detect ammonia selectively in the presence of other gases, such as those tested in this work. Note that the investigated interfering gases were taken at a much higher concentration compared with the ammonia.

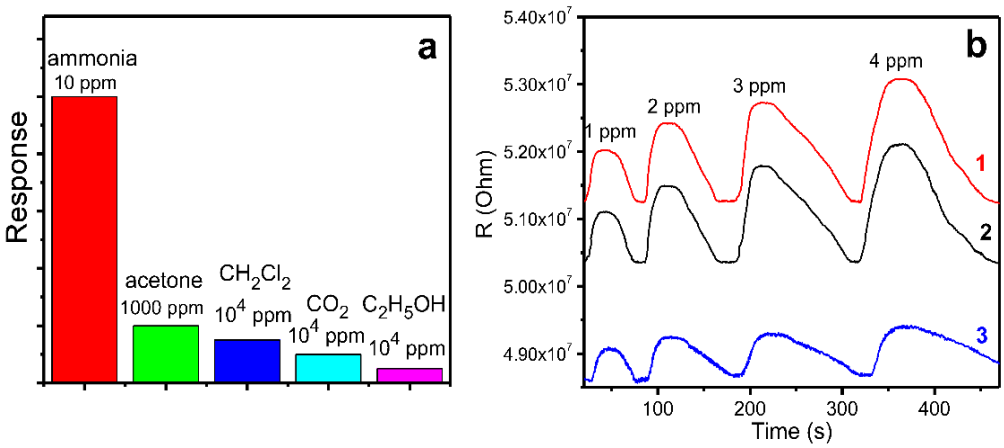

Figure 9. (**a**) Response of a $ZnPcF_4$ film to ammonia (10 ppm), acetone (1000 ppm), dichloromethane (10^4 ppm), carbon dioxide (10^4 ppm), and ethanol (10^4 ppm); (**b**) Response of a $ZnPcF_4$ film to ammonia (1–4 ppm) in air measured at relative humidity of 5% (1), 30% (2), and 70% (3).

The dependence of the sensor response on the relative humidity (RH) was also examined and the results are presented in Figure 9b, which show that the initial resistance of the $ZnPcF_4$ films decreases with the increase of RH from 5% to 70%. The value of the sensor response to NH_3 at RH 5% and 30% is almost the same, however, it is found to decrease noticeably when increasing the RH to 70%. The main

reason for such behavior appears to be a competitive sorption of the NH_3 and H_2O molecules on the surface of the $ZnPcF_4$ film.

The sensor response of a $ZnPcF_4$ layer toward ammonia in the air was also compared with that in a mixture of gases, with the composition close to the exhaled air of healthy people. Figure 7b shows that the value of the sensor response to NH_3 in the presence of gas mixture (N_2 76%, O_2 16%, H_2O 5%, and CO_2 3%) is almost the same as in the mixture with air. This makes the $ZnPcF_4$ films a promising sensing layer for the detection of ammonia in exhaled air, which is used as a gas-biomarker of renal failure in nephritis, atherosclerosis of the renal arteries, and toxic affections of the kidneys [3].

Note that the sensor performance of several sensors towards ammonia has been reported in the literature [48–53]. Some examples of sensor characteristics of several sensors, including the data obtained in this work, are summarized in Table 3 for comparison.

Table 3. Sensor performance of active layers based on metal oxides, conducting polymers, carbon-containing nanomaterials, and phthalocyanines.

Sensing Layer	Concentration Range, ppm	Minimal Investigated Concentration, ppm	Response/ Recovery Time, s	Temperature Range, °C	Ref.
Metal Oxides					
Pt/NiO	1–1000	0.01	15/76 (350 °C, 1000 ppm)	200–350	[7]
Pt Nanoparticle/Aluminum-Doped Zinc Oxide	1–1000	1	24/4 (350 °C, 1000 ppm)	200–350	[48]
Conducting Polymers					
Polyaniline/poly(styrene-butadiene-styrene)	0.1–100	0.1	≤13 (100 ppm)/–	Room temperature	[49]
Flexible polyaniline films	50–150	50	40 (50 ppm)/–	Room temperature	[50]
Carbon-Containing Nanomaterials and Phthalocyanines					
AuNPs/SWNT	0.25–6	0.255	20 (0.4 ppm)/–	Room temperature	[51]
rGO modified with metal tetra-α-iso-pentyloxyme-tallophthalocyanines (CuPc, NiPc, PbPc)	0.4–400	0.4	CuPc/rGO 364/115 NiPc/rGO 200/264 PbPc/rGO 248/331 (0.8 ppm)	Room temperature	[52]
CoPc on a flexible polyethylene terephthalate substrate	5–50	5	25/156 (20 ppm)	Room temperature	[53]
$ZnPcF_4$	0.1–50	0.1	25/110 (10 ppm)	Room temperature	This work

The sensing layers based on $ZnPcF_4$ are quite competitive with the active layers, based on metal oxides, conducting polymers, and carbon-containing nanomaterials, described in the literature; the $ZnPcF_4$ films exhibit a reversible sensor response at room temperature, a low detection limit, and low values of response and recovery times, compared with the other sensors.

4. Conclusions

In this work, unsubstituted metal phthalocyanines (MPc, M = Cu, Co, Zn), tetrafluorosubstituted metal phthalocyanines ($MPcF_4$) and hexadecafluorosubstituted metal phthalocyanines ($MPcF_{16}$) thin films were deposited by organic molecular beam deposition and studied, to reveal the effects of the central metals and F-substituents on the films' sensor response to ammonia.

It has been shown that the sensor response decreased in the order of $CoPcF_x > ZnPcF_x > CuPcF_x$, both in the case of the unsubstituted and fluorinated derivatives. The sensor response of the $MPcF_4$ films to ammonia is noticeably higher than that of the MPc films, which is in good correlation with the

values of the binding energy between the metal phthalocyanine and NH_3 molecule, as calculated by the DFT method. At the same time, in contrast to the DFT calculations, $MPcF_{16}$ demonstrated the lesser sensor response compared with $MPcF_4$, which appeared to be connected with the different structure and morphology of their films.

It has been shown, using $ZnPcF_4$ films as an example, that they exhibit a sensitivity to ammonia, up to concentrations as low as 0.1 ppm, and can be used for the selective detection of ammonia in the presence of some reducing gases and volatile organic compounds. Moreover, the $ZnPcF_4$ films can be used for the detection of NH_3 in the gas mixture simulating exhaled air (N_2 76%, O_2 16%, H_2O 5%, and CO_2 3%). This makes these films promising active layers as chemiresistive sensors for the detection of ammonia in exhaled air, which is a biomarker of some kidney diseases.

Author Contributions: Conceptualization, T.B.; methodology, P.K.; validation, D.K., A.S., S.G., and T.B.; formal analysis, A.S.; investigation, D.K. and A.S.; writing (original draft preparation), D.K. and T.B.; writing (review and editing), T.B.; visualization, A.S.; supervision, S.G.; project administration, T.B.; funding acquisition, T.B.

Funding: This research was funded by the FASO of the Russian Federation (project 0300-2016-0007).

Acknowledgments: The authors are grateful to the Data-Computing Center of Novosibirsk State University for the provision supercomputer facility.

Conflicts of Interest: The authors declare no conflict of interest. The funders had no role in the design of the study; in the collection, analyses, or interpretation of data; in the writing of the manuscript, and in the decision to publish the results.

References

1. Timmer, B.; Olthuis, W.; van den Berg, A. Ammonia sensors and their applications: A review. *Sens. Actuators B* **2005**, *107*, 666–677. [CrossRef]
2. Di Natale, C.; Paolesse, R.; Martinelli, E.; Capuano, R. Solid-state gas sensors for breath analysis: A review. *Anal. Chim. Acta* **2014**, *824*, 1–17. [CrossRef] [PubMed]
3. DuBois, S.; Eng, S.; Bhattacharya, R.; Rulyak, S.; Hubbard, T.; Putnam, D.; Kearney, D. Breath Ammonia Testing for Diagnosis of Hepatic Encephalopathy. *Dig. Dis. Sci.* **2005**, *50*, 1780–1784. [CrossRef] [PubMed]
4. Mount, G.H.; Rumberg, B.; Havig, J.; Lamb, B.; Westberg, H.; Yonge, D.; Johson, K.; Kincaid, R. Measurement of atmospheric ammonia at a dairy using differential optical absorption spectroscopy in the mid-ultraviolet. *Atmos. Environ.* **2002**, *36*, 1799–1810. [CrossRef]
5. Jin, Z.; Su, Y.; Duan, Y. Development of a polyaniline-based optical ammonia sensor. *Sens. Actuators B* **2001**, *72*, 75–79. [CrossRef]
6. Lee, Y.-S.; Joo, B.-S.; Choi, N.-J.; Lim, J.-O.; Huh, J.-S.; Lee, D.-D. Visible optical sensing of ammonia based on polyaniline film. *Sens. Actuators B* **2003**, *93*, 148–152. [CrossRef]
7. Chen, H.-I.; Hsiao, C.-Y.; Chen, W.-C.; Chang, C.-H.; Chou, T.-C.; Liu, I.-P.; Lin, K.-W.; Liu, W.-C. Characteristics of a Pt/NiO thin film-based ammonia gas sensor. *Sens. Actuators B* **2018**, *256*, 962–967. [CrossRef]
8. Joshi, N.; Hayasaka, T.; Liu, Y.; Liu, H.; Oliveira, O.N., Jr.; Lin, L. A review on chemiresistive room temperature gas sensors based on metal oxide nanostructures, graphene and 2D transition metal dichalcogenides. *Microchim. Acta* **2018**, *185*, 213. [CrossRef] [PubMed]
9. Kumar, L.; Rawal, I.; Kaur, A.; Annapoorni, S. Flexible room temperature ammonia sensor based on polyaniline. *Sens. Actuators B* **2017**, *240*, 408–416. [CrossRef]
10. Park, S.J.; Park, C.S.; Yoon, H. Chemo-Electrical Gas Sensors Based on Conducting Polymer Hybrids. *Polymers* **2017**, *9*, 155. [CrossRef]
11. Wang, Q.; Wu, S.; Ge, F.; Zhang, G.; Lu, H.; Qiu, L. Solution-Processed Microporous Semiconductor Films for High-Performance Chemical Sensors. *Adv. Mater. Interfaces* **2016**, *3*, 1600518. [CrossRef]
12. Pandey, S. Highly sensitive and selective chemiresistor gas/vapor sensors based on polyaniline nanocomposite: A comprehensive review. *J. Sci. Adv. Mater. Devices* **2016**, *1*, 431–453. [CrossRef]
13. Crowley, K.; Morrin, A.; Hernandez, A.; O'Malley, E.; Whitten, P.G.; Wallace, G.G.; Smytha, M.R.; Killard, A.J. Fabrication of an ammonia gas sensor using inkjet-printed polyaniline nanoparticles. *Talanta* **2008**, *77*, 710–717. [CrossRef]

14. Wannebroucq, A.; Gruntz, G.; Suisse, J.-M.; Nicolas, Y.; Meunier-Prest, R.; Mateos, M.; Toupance, T.; Bouvet, M. New n-type molecular semiconductor-doped insulator (MSDI) heterojunctions combining a triphenodioxazine (TPDO) and the lutetium bisphthalocyanine ($LuPc_2$) for ammonia sensing. *Sens. Actuators B* **2018**, *255*, 1694–1700. [CrossRef]
15. Klyamer, D.D.; Sukhih, A.S.; Krasnov, P.O.; Gromilov, S.A.; Morozova, N.B.; Basova, T.V. Thin films of tetrafluorosubstituted cobalt phthalocyanine: Structure and sensor properties. *Appl. Surf. Sci.* **2016**, *372*, 79–86. [CrossRef]
16. Sukhikh, A.S.; Klyamer, D.D.; Parkhomenko, R.G.; Krasnov, P.O.; Gromilov, S.A.; Hassan, A.K.; Basova, T.V. Effect of fluorosubstitution on the structure of single crystals, thin films and spectral properties of palladium phthalocyanines. *Dyes Pigment.* **2018**, *149*, 348–355. [CrossRef]
17. Hesse, K.; Schlettwein, D. Spectroelectrochemical investigations on the reduction of thin films of hexadecafluorophthalocyaninatozinc ($F_{16}PcZn$). *J. Electroanal. Chem.* **1999**, *476*, 148–158. [CrossRef]
18. Engel, M.K. Single-Crystal Structures of Phthalocyanine Complexes and Related Macrocycles. In *The Porphyrin Handbook*; Kadish, K.M., Smith, K.M., Guilard, R., Eds.; Academic Press: San Diego, CA, USA, 2003; Volume 20, pp. 1–242. ISBN 0-12-39322.
19. Schollhorn, B.; Germain, J.P.; Pauly, A.; Maleysson, C.; Blanc, J.P. Influence of peripheral electron-withdrawing substituents on the conductivity of zinc phthalocyanine in the presence of gases. Part 1: Reducing gases. *Thin Solid Films* **1998**, *326*, 245–250. [CrossRef]
20. Ma, X.; Chen, H.; Shi, M.; Wu, G.; Wang, M.; Huang, J. High gas-sensitivity and selectivity of fluorinated zinc phthalocyanine film to some non-oxidizing gases at room temperature. *Thin Solid Films* **2005**, *489*, 257–261. [CrossRef]
21. Brinkmann, H.; Kelting, C.; Makarov, S.; Tsaryova, O.; Schnurpfeil, G.; Wöhrle, D.; Schlettwein, D. Fluorinated phthalocyanines as molecular semiconductor thin films. *Phys. Status Solidi A* **2008**, *205*, 409–420. [CrossRef]
22. Becke, A.D. Density-functional exchange energy approximation with correct asymptotic behavior. *Phys. Rev. A* **1988**, *88*, 3098–3100. [CrossRef]
23. Perdew, J.P. Density functional approximation for the correlation energy of the inhomogeneous electron gas. *Phys. Rev. B* **1986**, *33*, 8822–8824. [CrossRef]
24. Schaefer, A.; Horn, H.; Ahlrichs, R. Fully optimized contracted Gaussian basis set for atoms Li to Kr. *J. Chem. Phys.* **1992**, *97*, 2571–2577. [CrossRef]
25. Schaefer, A.; Huber, C.; Ahlrichs, R. Fully optimized contracted Gaussian basis set of triple zeta valence quality for atoms Li to Kr. *J. Chem. Phys.* **1994**, *100*, 5829–5835. [CrossRef]
26. Grimme, S.; Ehrlich, S.; Goerigk, L. Effect of the Damping Function in Dispersion Corrected Density Functional Theory. *J. Comput. Chem.* **2011**, *32*, 1456–1465. [CrossRef] [PubMed]
27. Grimme, S.; Antony, J.; Ehrlich, S.; Krieg, H. A consistent and accurate ab initio parametrization of density functional dispersion correction (DFT-D) for the 94 elements H-Pu. *J. Chem. Phys.* **2010**, *132*, 154104. [CrossRef] [PubMed]
28. Neese, F. The ORCA program system, WIREs. *Comput. Mol. Sci.* **2012**, *2*, 73–78. [CrossRef]
29. Mulliken, R.S. Electronic Population Analysis on LCAO–MO Molecular Wave Functions. I. *J. Chem. Phys.* **1955**, *23*, 1833–1840. [CrossRef]
30. Mulliken, R.S. Electronic Population Analysis on LCAO–MO Molecular Wave Functions. II. Overlap Populations, Bond Orders, and Covalent Bond Energies. *J. Chem. Phys.* **1955**, *23*, 1841–1846. [CrossRef]
31. Mayer, I. Bond order and valence—Relations to Mulliken population analysis. *Int. J. Quant. Chem.* **1984**, *26*, 151–154. [CrossRef]
32. Mayer, I. Bond orders and valences in the SCF theory—A comment. *Theor. Chim. Acta* **1985**, *67*, 315–322. [CrossRef]
33. Liang, X.; Chen, Z.; Wu, H.; Guo, L.; He, C.; Wang, B.; Wu, Y. Enhanced NH_3-sensing behavior of 2,9,16,23-tetrakis(2,2,3,3-tetrafluoropropoxy) metal(II) phthalocyanine/multi-walled carbon nanotube hybrids: An investigation of the effects of central metals. *Carbon* **2014**, *80*, 268–278. [CrossRef]
34. Tang, Q.; Li, H.; Liu, Y.; Hu, W. High-performance air-stable n-type transistors with an asymmetrical device configuration based on organic single-crystalline submicrometer/nanometer ribbons. *J. Am. Chem. Soc.* **2006**, *128*, 14634–14639. [CrossRef] [PubMed]
35. Barsan, N.; Simion, C.; Heine, T.; Pokhrel, S.; Weimar, U. Modeling of sensing and transduction for p-type semiconducting metal oxide based gas sensors. *J. Electroceram.* **2010**, *25*, 11–19. [CrossRef]

36. Kim, H.-J.; Lee, J.-H. Highly sensitive and selective gas sensors using p-type oxide semiconductors: Overview. *Sens. Actuators B* **2014**, *192*, 607–627. [CrossRef]
37. Kerp, H.R.; Westerdui, K.T.; van Veen, A.T.; van Faassen, E.E. Quantification and effects of molecular oxygen and water in zinc phthalocyanine layers. *J. Mater. Res.* **2001**, *16*, 503–511. [CrossRef]
38. De Haan, A.; Debliquy, M.; Decroly, A. Influence of atmospheric pollutants on the conductance of phthalocyanine films. *Sens. Actuators B Chem.* **1999**, *57*, 69–74. [CrossRef]
39. Gould, R.D. Structure and electrical conduction properties of phthalocyanine thin films. *Coord. Chem. Rev.* **1996**, *156*, 237–274. [CrossRef]
40. Schlettwein, D.; Graaf, H.; Meyer, J.-P.; Oekermann, T.; Jaeger, N.I. Molecular interactions in thin films of hexadecafluorophthalocyaninatozinc (F_{16}PcZn) as compared to islands of *N*,*N*′-dimethylperylene-3,4,9,10-biscarboximide (MePTCDI). *J. Phys. Chem. B* **1999**, *103*, 3078–3086. [CrossRef]
41. Schlettwein, D.; Hesse, K.; Gruhn, N.E.; Lee, P.A.; Nebesny, K.W.; Armstrong, N.R. Electronic energy levels in individual molecules, thin films, and organic heterojunctions of substituted phthalocyanines. *J. Phys. Chem. B* **2001**, *105*, 4791–4800. [CrossRef]
42. Parkhomenko, R.G.; Sukhikh, A.S.; Klyamer, D.D.; Krasnov, P.O.; Gromilov, S.A.; Kadem, B.; Hassan, A.K.; Basova, T.V. Thin films of unsubstituted and fluorinated palladium phthalocyanines: Structure and sensor response toward ammonia and hydrogen. *J. Phys. Chem. C* **2017**, *121*, 1200–1209. [CrossRef]
43. Erk, P.; Hengelsberg, H.; Haddow, M.F.; van Gelder, R. The innovative momentum of crystal engineering. *CrystEngComm* **2004**, *6*, 474–483. [CrossRef]
44. Ballirano, P.; Caminiti, R.; Ercolani, C.; Maras, A.; Orru, M.A. X-ray powder diffraction structure reinvestigation of the α and β forms of cobalt phthalocyanine and kinetics of the α → β phase transition. *J. Am. Chem. Soc.* **1998**, *120*, 12798–12807. [CrossRef]
45. Vergnat, C.; Landais, V.; Legrand, J.-F.; Brinkmann, M. Orienting semiconducting nanocrystals on nanostructured polycarbonate substrates: Impact of substrate temperature on polymorphism and in-plane orientation. *Macromolecules* **2011**, *44*, 3817–3827. [CrossRef]
46. Pandey, P.A.; Rochford, L.A.; Keeble, D.S.; Rourke, J.P.; Jones, T.S.; Beanland, R.; Wilson, N.R. Resolving the nanoscale morphology and crystallographic structure of molecular thin films: F_{16}CuPc on graphene oxide. *Chem. Mater.* **2012**, *24*, 1365–1370. [CrossRef]
47. Yoon, S.M.; Song, H.J.; Hwang, I.-C.; Kim, K.S.; Choi, H.C. Single crystal structure of copper hexadecafluorophthalocyanine (F_{16}CuPc) ribbon. *Chem. Commun.* **2010**, *46*, 231–233. [CrossRef] [PubMed]
48. Chen, H.-I.; Chi, C.-Y.; Chen, W.-C.; Liu, I.-P.; Chang, C.-H.; Chou, T.-C.; Liu, W.-C. Ammonia Sensing Characteristic of a Pt Nanoparticle/Aluminum-Doped Zinc Oxide Sensor. *Sens. Actuators B* **2018**, *267*, 145–154. [CrossRef]
49. Wang, X.; Meng, S.; Tebyetekerwa, M.; Weng, W.; Pionteck, J.; Sun, B.; Qin, Z.; Zhu, M. Nanostructured polyaniline/poly(styrene-butadiene-styrene) composite fiber for use as highly sensitive and flexible ammonia sensor. *Synth. Met.* **2017**, *233*, 86–93. [CrossRef]
50. Matindoust, S.; Farzi, A.; Nejad, M.B.; Abadi, M.H.S.; Zou, Z.; Zheng, L.R. Ammonia gas sensor based on flexible polyaniline films for rapid detection of spoilage in protein-rich foods. *J. Mater. Sci. Mater. Electron.* **2017**, *28*, 7760–7768. [CrossRef]
51. Lee, K.; Scardaci, V.; Kim, H.-Y.; Hallam, T.; Nolan, H.; Bolf, B.E.; Maltbie, G.S.; Abbott, J.E.; Duesberg, G.S. Highly sensitive, transparent, and flexible gas sensors based on gold nanoparticle decorated carbon nanotubes. *Sens. Actuators B* **2013**, *188*, 571–575. [CrossRef]
52. Li, X.; Wang, B.; Wang, X.; Zhou, X.; Chen, Z.; He, C.; Yu, Z.; Wu, Y. Enhanced NH_3-Sensitivity of Reduced Graphene Oxide Modified by Tetra-α-Iso-Pentyloxymetallophthalocyanine Derivatives. *Nanoscale Res. Lett.* **2015**, *10*, 373. [CrossRef] [PubMed]
53. Singh, A.; Kumar, A.; Kumar, A.; Samanta, S.; Joshi, N.; Balouria, V.; Debnath, A.K.; Prasad, R.; Salmi, Z.; Chehimi, M.M.; et al. Bending stress induced improved chemiresistive gas sensing characteristics of flexible cobalt-phthalocyanine thin films. *Appl. Phys. Lett.* **2013**, *102*, 132107. [CrossRef]